Applied Catalysis B: Environmental 134–135 (2013) 60–65

Contents lists available at SciVerse ScienceDirect

Applied Catalysis B: Environmental

journal homepage: www.elsevier.com/locate/apcatb

# The replacement of {1 0 1} by {0 1 0} facets inhibits the photocatalytic activity of anatase $TiO_2$

Liqun Ye, Jinyan Liu, Lihong Tian, Tianyou Peng, Ling Zan*

*College of Chemistry and Molecular Science, Wuhan University, Wuhan 430072, People's Republic of China*

ARTICLE INFO

*Article history:*
Received 31 October 2012
Received in revised form
25 December 2012
Accepted 30 December 2012
Available online 9 January 2013

*Keywords:*
$TiO_2$
Photocatalytic
Facet
Time-resolved PL

ABSTRACT

Anatase $TiO_2$ crystals with {1 0 1}–{0 0 1} and {0 1 0}–{0 0 1} two facets coexistence were synthesized by $(NH_4)_2TiF_6$ acting as titanium and fluorine sources and the photocatalytic activity of the samples were investigated. The replacement of {1 0 1} by {0 1 0} facets inhibits the photocatalytic activity of anatase $TiO_2$. The mechanism was examined by photoluminescence spectrum, time-resolved photoluminescence spectra, field emission scanning electron microscope (FESEM) images of selected deposition of Ag, surface atoms structures and electronic band structures of anatase $TiO_2$ facets. The results demonstrated that photoinduced charge transfer properties between {1 0 1} facets and {0 0 1} facets resulted in the efficient charge separation. Replacing {1 0 1} by {0 1 0}, the charge transfer mechanism was altered and the photoinduced electron–hole pairs cannot be separated well. The photocatalytic activity of it has thus been inhibited.



## 1. Introduction

$TiO_2$ is the most widely applied semiconductor photocatalyst, used in almost all of environment and energy photocatalysis, demonstrating promising conversion values [1–3]. As an important feature of crystalline materials, crystal facets of $TiO_2$ having different atomic arrangement and electronic structures exhibit different intrinsic reactivity and surface physical/chemical properties [4,5]. Since *Yang*'s report [6] about anatase $TiO_2$ properties with dominant {0 0 1} facets, the facet-dependent photocatalytic activity of anatase has been intensively investigated [7–16]. At the beginning, the researchers suggested, based on theoretical calculations, that the {0 0 1} facets are the photocatalytic active facets and the {0 0 1} facets have higher reactivity compared to the {1 0 1} facets, due to its higher concentration of low coordination Ti5c centers and high surface energy [7,8]. Recent investigations further revealed that $TiO_2$ with {1 0 1}–{0 0 1} two facets coexistence exhibited even better photocatalytic activity than that of the dominant {0 0 1} facets [9,17,18]. For instances, Liu and Gordon found that the photocatalytic reduction activity of {1 0 1} facets was greater than that of {0 0 1} facets for photocatalytic $H_2$ evolution [9,16]. *Huang* reported that $TiO_2$ with (55%) {1 0 1} and (45%) {0 0 1} displayed a higher photocatalytic oxidation and reduction activity than the sample with dominant exposed {0 0 1} facets [17]. Furthermore, single-molecule imaging analysis and photogenerated defect analysis indicated that the photoinduced electrons incline to transfer to {1 0 1} facets and hole to {0 0 1} facets when {1 0 1}–{0 0 1} two facets coexist, and an efficient charge separation can be expected in such circumstance [19–24]. It suggests that the higher photocatalytic activity of anatase $TiO_2$ is from the synergism of {1 0 1} and {0 0 1} facets, i.e., the coexistence of {1 0 1} with {0 0 1} facets enhances the photocatalytic activity.

There are three fundamental low-index facets: {1 0 1}, {0 0 1}, and {0 1 0} exposed in $TiO_2$ crystals, as shown in Scheme 1. The photocatalytic activity of $TiO_2$ can be tailored by fine-tuning the particle morphology and, specifically, the exposed specific crystal facets [7–16]. To the best of our knowledge, there are only few reports about the photocatalytic activity of anatase $TiO_2$, in which {0 1 0} facets coexisting with {0 0 1} facets.

In this paper, 1 0 1/0 0 1 – 1 (49% {0 0 1} and 51% {1 0 1}), 1 0 1/0 0 1 – 2 (70% {0 0 1} and 30% {1 0 1}), 0 1 0/0 0 1 – 1 (48% {0 0 1} and 52% {0 1 0}) and 0 1 0/0 0 1 – 2 (64% {0 0 1} and 36% {0 1 0}) anatase $TiO_2$ samples were synthesized. In analyzing the generation of photocatalytic reactive oxygen species (hydroxy radical, $^{\bullet}OH$ and superoxide radical, $O_2^{\bullet-}$), we found that the replacement of {1 0 1} by {0 1 0} facets inhibited the photocatalytic activity of anatase $TiO_2$. The reasons were well explained with PL spectrum, SEM images of selected deposition of Ag, surface atoms structures and electronic band structures of anatase $TiO_2$ facets.

## 2. Experimental

### 2.1. Materials and synthesis

Ammonium hexafluorotitanate ($(NH_4)_2TiF_6$), tetrabutyl titanate, hydrochloric acid (HCl), terephthalic acid (TA), nitroblue

* Corresponding author.
*E-mail address:* irlab@whu.edu.cn (L. Zan).

0926-3373/$ – see front matter © 2013 Elsevier B.V. All rights reserved.
http://dx.doi.org/10.1016/j.apcatb.2012.12.043

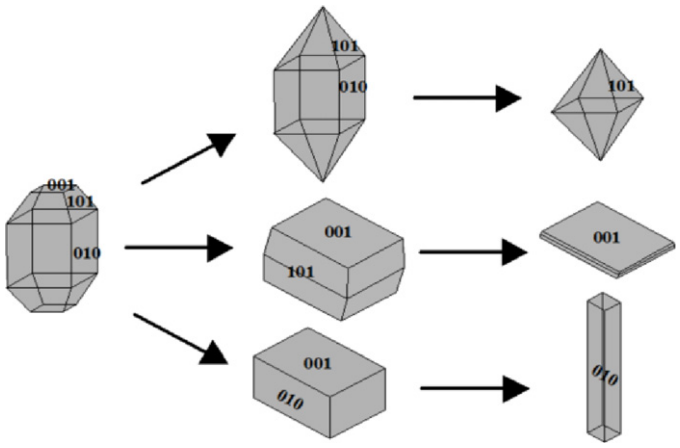


**Scheme 1.** Schematic drawings of anatase $TiO_2$ shapes.

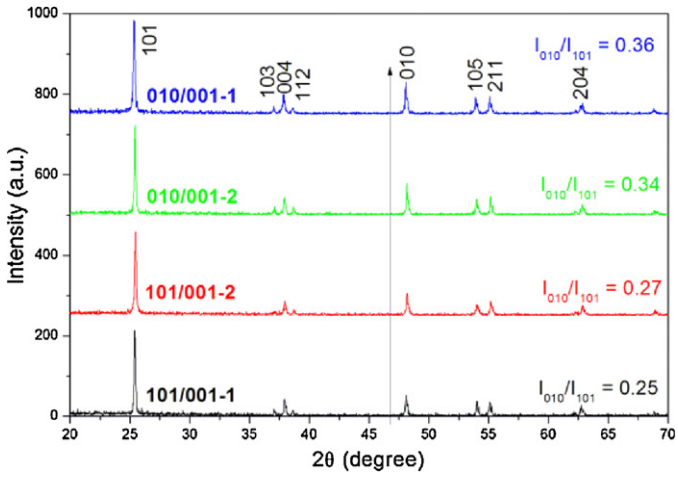


**Fig. 1.** XRD patterns of $TiO_2$ samples.

tetrazolium (NBT) and ethanol are analytical pure and from Sinopharm Chemical Reagent Co., Ltd.

A mixture of deionized water and concentrated HCl (36.5% by weight) in total volume of 30 mL was stirred at ambient conditions for 5 min in a Teflon-lined stainless-steel autoclave (40 mL volume), and 1 mL of tetrabutyl titanate and 0.25 g $(NH_4)_2TiF_6$ were added into the solution and stirred for another 5 min. The hydrothermal synthesis was conducted at 150–180 °C for 24 h in a muffle furnace. After synthesis, the autoclave was cooled down, all samples were filtered and washed by deionized water (pH 7.00) several times and then dried at 80 °C for 12 h. And then all samples were heated at 600 °C for 2 h to remove surface-fluorine. For 101/001 – 1, 101/001 – 2, 010/001 – 1 and 010/001 – 2, the volume ratio of hydrochloric acid to water was 10/20, 15/15, 10/20 and 15/15, respectively. The hydrothermal temperature was 180 °C, 180 °C, 150 °C and 150 °C, respectively.

### 2.2. Characterization

X-ray diffraction patterns (XRD) of the samples recorded at room temperature, by a Bruker D8 advance X-ray diffractometer using Cu Kα radiation and 2θ scan rate of 4° $min^{-1}$. Diffraction patterns were taken over the 2θ range 20–70°. FESEM images were obtained by a JEOL JEM-6700F Field Emission Scanning Electron Microscope with operating at an accelerating voltage and applied current of 15 kV and 10 mA, respectively. X-ray photoelectron spectroscopy (XPS) measurements were carried out by a VG Multilab 2000 spectrometer (Thermo Electron Corporation) with an Mg Kα X-ray source, and the spectra calibrated to the C1s peak at 284.6 eV. Photoluminescence (PL) spectra of $TiO_2$ powders were obtained on a Jasco FP-6500 with $\lambda_{exc}$ = 320 nm. Time-resolved PL spectra recorded at 398 nm with 330 nm excitation at room temperature, by a FLS920 Multifunction Steady State and Transient State Fluorescence Spectrometer (Edinburgh Instruments). Raman spectra of samples were recorded on a confocal Raman microspectroscopy (RM-1000) with 514.5 nm laser excitation. The Brunauer–Emmett–Teller (BET) surface areas were measured using quantachrome autosorb-1 automated gas sorption systems at 77 K.

### 2.3. Photoactivity test

The photoactivity was evaluated under UV light (λ = 365 nm) irradiation. The UV light was emitted by a 300 W high pressure xenon lamp (Changzhou Yuyu Electro-Optical Device Co., Ltd. China). Typical photocatalytic process is arranged in such a way: 100 mL aqueous suspensions of substrate (TA ($5 \times 10^{-4}$ mol/L) and NaOH ($2 \times 10^{-3}$ mol/L) solution; NBT ($5 \times 10^{-5}$ mol/L) solution) placed in a quartz beaker and then 20 mg photocatalysts were added. Prior to irradiation, the suspensions were sonicated for 10 min and then magnetically stirred in dark for 30 min to get desorption–adsorption equilibrium. The suspensions were kept under constant air-equilibrated conditions during irradiation. A magnetic stirrer was employed for continuous mixing. At certain time intervals, 4 mL suspensions were sampled and centrifuged by TGL-16G centrifuge (Shanghai Anting Scientific Instrument Factory, China) at 10,000 rpm for 15 min to remove the particles. The upper clear liquid of NBT was analyzed by recording the maximum absorption band (259 nm for NBT) and UV–vis spectra of NBT using a Shimadzu UV-3600 spectrophotometer. The upper clear liquid of TA was analyzed by recording the maximum PL peak (426 nm for TAOH) and PL spectra using a Jasco FP-6500 with $\lambda_{exc}$ = 315 nm.

## 3. Results and discussion

### 3.1. Catalyst characterization

Fig. 1 shows the XRD patterns of $TiO_2$ samples. The peaks located at 25.4° (101), 37.8° (004), 48.5° (200), 54.0° (105), 55.4° (211) and 62.9° (204) are indexed to that of anatase $TiO_2$ with the tetragonal structure (JCPDS file No. 73-2062, space group I41/amd), demonstrating the formation of pure anatase $TiO_2$. On the other hand, it can be seen that the intensity of (010) peak and I010/I101 increase in the order of 010/001 – 1 > 010/001 – 2 > 101/001 – 2 > 101/001–1 (Fig. S1), implying 010/001 – 1 and 010/001 – 2 have more {010} facets [25].

Fig. 2 shows the FESEM images of $TiO_2$ samples. For 101/001 – 1 (Fig. 1(a) and (b)), it has a size of about 600 nm and the thickness is about 130 nm. According to the symmetries of anatase $TiO_2$ crystals, the two flat and square surfaces should be {001} facets and the eight hexagonal surfaces are {101} facets, respectively. An angle of 112°, consistent with the interfacial angle between {001} and {101} facets, was observed on the particles. It suggested the coexistence of {001} and {101} facets in sample 101/001 – 1. For 101/001 – 2 (Fig. 2(c) and (d)), the geometry configuration is similar to 101/001 – 1, which also exhibit flat facets of {001} and {101}. But the size and thickness decrease to around 500 nm and 50 nm, respectively. The Fig. 2e gives a schematic illustration of 101/001 – 1 sample.

For 010/001 – 1 (Fig. 2(f) and (g)), it has a size of around 800 nm and the thickness of about 220 nm. The geometry configuration is different from 101/001 – 1 and 101/001 – 2. There are rectangle

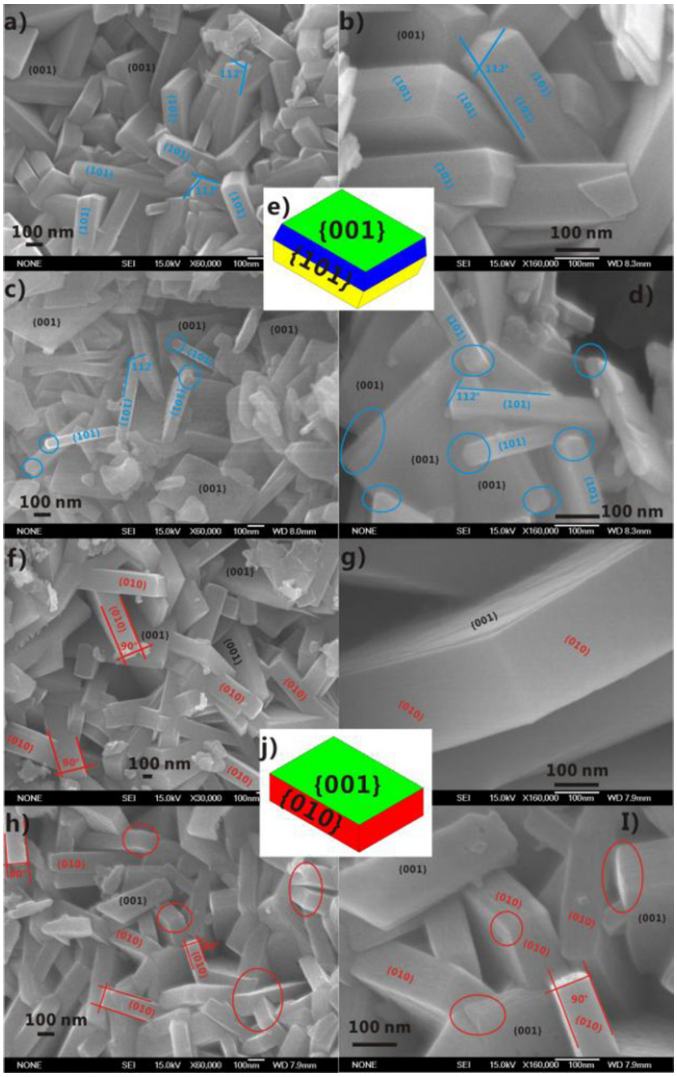


**Fig. 2.** (a) and (b): FESEM images of 101/001–1; (c) and (d): FESEM images of 101/001–2; (e) scheme of 101/001 samples; (f) and (g): FESEM images of 010/001–1; (h) and (i): FESEM images of 010/001–2; and (j) scheme of 010/001 samples.

flat facets instead of the hexagonal {1 0 1} facets. The interfacial angle between square facets and rectangle facets is 90°. According to the symmetries of anatase $TiO_2$ crystals, the two flat and square surfaces should be {0 0 1} facets and the four rectangle flat facets are {0 1 0} facets, respectively. For 0 1 0/0 0 1 – 2 (Fig. 2(h) and (i)), the geometry configuration is similar to 0 1 0/0 0 1 – 1, which also exhibits flat facets of {0 0 1} and {0 1 0}. But the size and thickness decrease to around 700 nm and 80 nm, respectively. The scheme illustrations of 1 0 1/0 0 1 – 1 and 1 0 1/0 0 1 – 2 samples are shown in Fig. 2j.

It can be found that the most of the particles are aggregated or even fused with each other via {0 0 1} facets (Fig. 2). Therefore, the real percentage of {0 0 1} exposed of as-synthesized samples are lower than the calculated data using idea single particle. Recently, *Tian* reported a new Raman Spectroscopy Technique to measure the {0 0 1} facets percentage of anatase $TiO_2$ [26] based on the experimental results and theoretical analysis, the {0 0 1} facets exposed percentage of anatase $TiO_2$ {0 0 1} could be determined via the peak intensity ratio of the $E_g$ and A1g peaks. Fig. 3 displays the Raman spectra of $TiO_2$ samples in this work. The B1g peak is caused by symmetric bending vibration of O—Ti—O at 394 $cm^{-1}$, the A1g peak belongs to antisymmetric bending vibration of O—Ti—O at 514 $cm^{-1}$ and the $E_g$ peak is mainly attributed to the symmetric

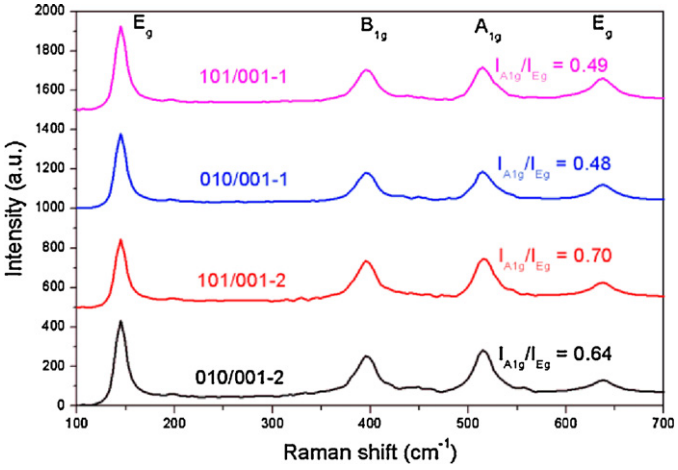


**Fig. 3.** Raman spectra in the range of 100–700 $cm^{-1}$ of $TiO_2$ samples.

stretching vibration of O—Ti—O in $TiO_2$ at 144 and 636 $cm^{-1}$ [9,26]. The {0 0 1} facets percentages of 101/001–1, 101/001–2, 010/001–1 and 010/001–2 were evaluated to be 49%, 70%, 48% and 64%, respectively.

The previous reports pointed out that the surface Ti—F bonds affect the photocatalytic activity of $TiO_2$ [7–16]. In order to avoid the influence of surface-fluorine in photocatalytic experiment, the anatase $TiO_2$ samples were heated at 600 °C for 2 h in a static air atmosphere to remove surface-fluorine and proved by XPS analysis. As shown in Fig. S2, the F-signal was negligible after the heat treatment.

### 3.2. Photocatalytic activity comparison

010/001–1 and 101/001–1 samples with similar {0 0 1} facet exposure and BET surface area (2.1 $m^2/g$ for 010/001–1, 2.3 $m^2/g$ for 101/001–1), were selected to study the affection of the photocatalytic activity of anatase $TiO_2$ as the replacement of {1 0 1} by {0 1 0} facets. Fig. 4 shows the intensity of the PL signal associated with 2-hydroxy terephthalic acid (TAOH) from the reaction of terephthalic acid (TA) with •OH (photocatalytic oxidation activity, Fig. 4a and Fig. S3) and transformation percentage of nitroblue tetrazolium (NBT) from the reaction of NBT with $O_2^{\bullet -}$ (photocatalytic reduction activity, Fig. 4b and Fig. S4) after 1 h irradiation of 0 1 0/0 0 1 –1 and 1 0 1/0 0 1 – 1 [27–29]. The results show that 101/001–1 possessed about 8 and 4 times higher photocatalytic oxidation and reduction activity respectively, in comparison to 010/001–1. Moreover, 101/001–2 (BET surface area: 10.4 $m^2/g$) also displayed higher photocatalytic oxidation and reduction activity than 010/001–2 (BET surface area: 8.6 $m^2/g$) (Fig. S5). These suggested the photocatalytic activity was repressed when {1 0 1} facets were replaced by {0 1 0} facets.

### 3.3. Photocatalytic mechanism

What is the origin of this inhibition when {1 0 1} replaced by {0 1 0} facets? Firstly, on the superficial level, the separation efficiency of photo-generated electron–hole is an important factor in a photocatalytic reaction. Photoluminescence (PL) emission mainly results from the recombination of excited electrons and holes, and lower PL intensity indicates a higher separation efficiency [30]. In Fig. 5a, two main peaks appear at about 398 (3.12 eV) and 468 nm (2.65 eV), respectively. Because the energy of former peak is nearly equal to the band gap (3.20 eV) of $TiO_2$, this emission can be attributed to the recombination of free electrons from the CB bottom to the recombination center at the ground state. The latter is

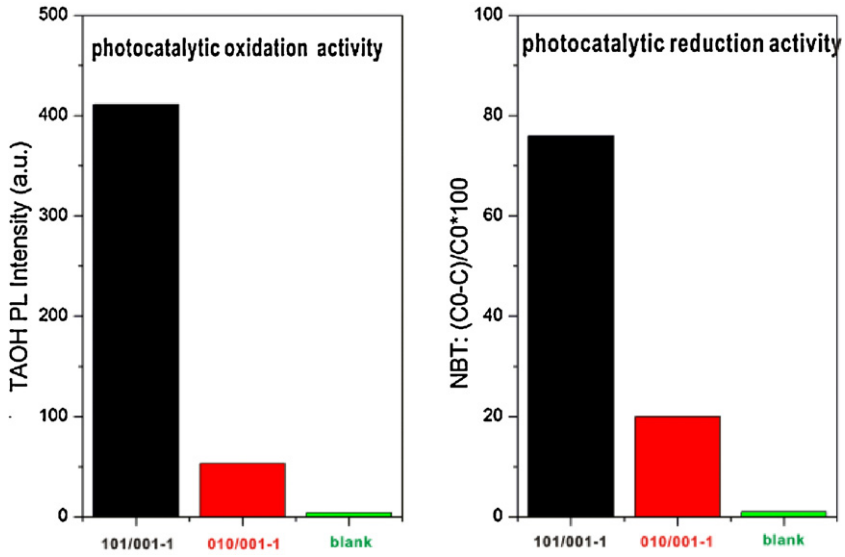


**Fig. 4.** Comparison of photocatalytic oxidation (a) and reduction (b) activity of 101/001–1 and 010/001–1.

the emission signal originating from the charge transfer transition from $Ti^{3+}$ to oxygen anions [5]. The PL intensity displays a significant increase when {1 0 1} facets were replaced by {0 1 0} facets, indicating that {1 0 1}–{0 0 1} samples have relatively low recombination rate of the photoinduced carriers than {0 1 0}–{0 0 1} samples under UV light irradiation. In addition, the lifetime of charge carriers was also reduced by {0 1 0} facets replacing the {1 0 1} facets. For instance, the lifetime of 010/001–1 is down to 5.84 ns, about 0.85 ns shorter than that of parent 101/001–1 (6.71 ns; Fig. 5b). This restricted lifetime also means the increased recombination rate of photoinduced carriers after the replacement of {1 0 1} by {0 1 0} facets.

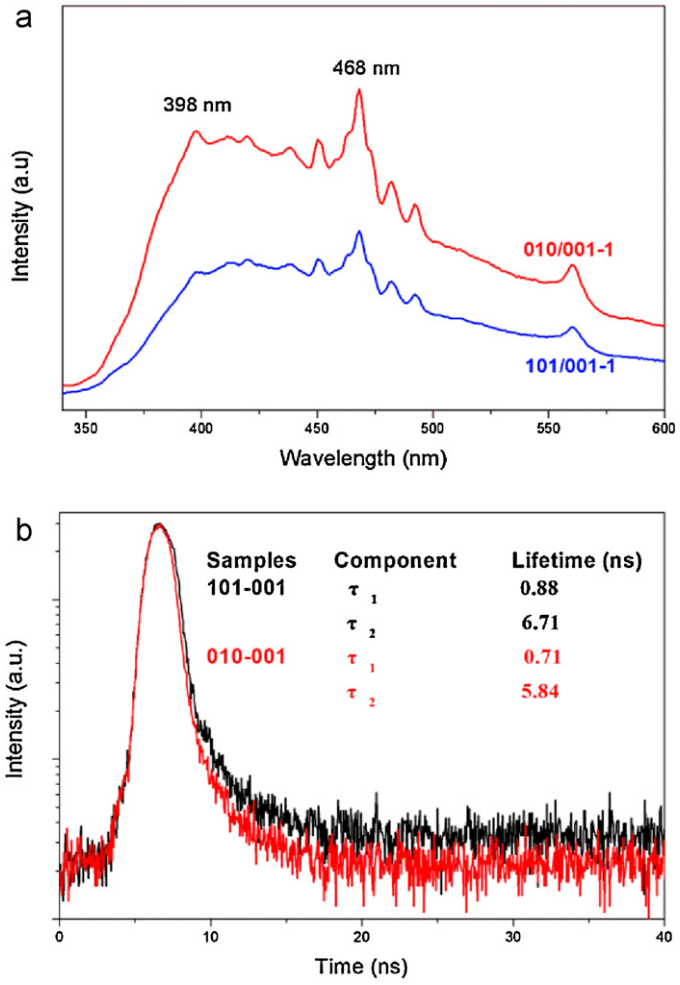


**Fig. 5.** (a) PL spectrum of 101/001–1 and 010/001–1; and (b) time-resolved PL spectra monitored at 398 nm with 330 nm excitation at 298 K for 101/001–1 and 010/001–1.

On the other hand, the linear relationship between the fluorescence intensity and irradiation time during 60 min was observed for 101/001–1, while the increment rate decreased after 30 min irradiation for 010/001–1 (Fig. S6). The increment amount of produced •OH per unit of time from the 101/001–1 monotonously increased as irradiation time increased up to 30 min, and then almost kept constant with further increase in irradiation time. Conversely, the increment amount of the •OH produced from 010/001–1 monotonously decreased with an increase in irradiation time. These results also demonstrated that the 101/001–1 can efficiently suppress the carrier recombination, but the photoinduced carrier recombination takes place for 010/001–1 [31]. In consequence, the replacement of {1 0 1} by {0 1 0} facets inhibited the photocatalytic activity of anatase $TiO_2$.

Secondly, on the deep level, different exposed facets have different arrangement and coordination of the surface atoms which result in the different valence band (VB) and conduction band (CB) energy levels. When the photoexcited electrons and holes diffuse from its bulk to the surface, the different energy levels of the conduction and valence bands drives the $e^-$ and $h^+$ to different crystal facets aiming to reach the most stable energy configuration. Namely, the VB and CB energy levels determine the transfer path of photoexcited holes and electrons, which can directly influence on the carrier separation efficiency [19,32].

Fig. S7 shows the atomic structural model of {1 0 1}, {0 0 1} and {0 1 0} facets. On the flat anatase {0 0 1} and {0 1 0} facets, all of the titanium atoms are unsaturated Ti5c atoms, and the angle of Ti—O—Ti are 146° and 156°, respectively. On the corrugated {1 0 1} facet, only half of the titanium atoms are unsaturated Ti5c atoms with a Ti—O—Ti angle of 102°. On the base of the different surface atomic structural of {1 0 1}, {0 0 1} and {0 1 0} facets, the CB and VB position are different. Theory calculations [17,32–34] showed that VB of three facets of $TiO_2$ crystals followed the order: {1 0 1} > {0 1 0} > {0 0 1}, and CB followed the order: {1 0 1} ≤ {0 0 1} ≤ {0 1 0}. In the latest progress,

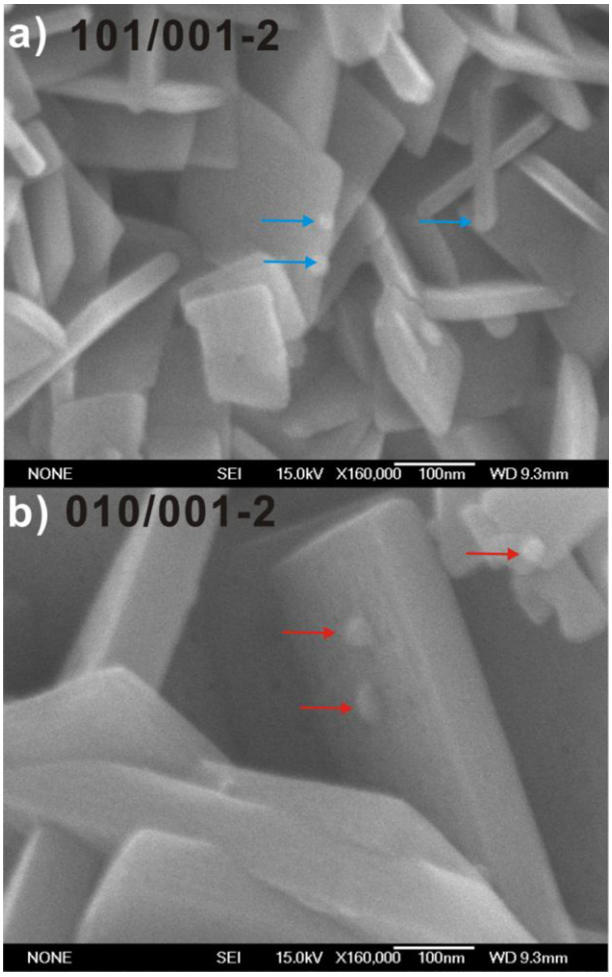


**Fig. 6.** FESEM images of Ag deposition of 101/001–2 and 010/001–2.

Tachikawa and Majima have fulfilled the orders of reduction and oxidation reactivity which support the theory calculation result [35].

For further confirming the electron transfer paths between {0 0 1} and {0 1 0} facets, {0 0 1} and {1 0 1} facets, Ag deposition was used. Fig. 6a shows the FESEM image of 101/001–2 photo-irradiated in silver nitrate solutions. Ag particles of a few nanometers in size were mainly observed on the {1 0 1} facets of 101/001–2. However, for 010/001–2, Ag nanoparticles were mainly observed on the {0 0 1} facets (Fig. 6b). This proves that most photoinduced electron transfer to {1 0 1} facets for {1 0 1}–{0 0 1} and {0 0 1} facets for {0 1 0}–{0 0 1} samples.

From the CB and VB energy level analyses and Ag deposition experiment, the relative CB and VB position of these samples were suggested as Scheme 2. For {1 0 1}–{0 0 1} samples (Scheme 2a), it can be found the photoinduced charge transfer tendency. Under UV light irradiation, the photoinduced electrons transfer to {1 0 1} facets and holes to {0 0 1} facets. Then, photocatalytic oxidation and reduction takes place on {0 0 1} and {1 0 1} facets, respectively (Scheme 2c). However, when {1 0 1} facets were replaced by {0 1 0} facets, the transfer scenario changed. The most electrons and holes transfer to {0 0 1} facets together and do not separate anymore under UV light irradiation (Scheme 2b). The photocatalytic oxidation and reduction are supposed occurring on {0 0 1} or {0 1 0} facets synchronously (Scheme 2d). The replacement of {1 0 1} by {0 1 0} facets is thus to inhibit the photocatalytic activity of anatase $TiO_2$.

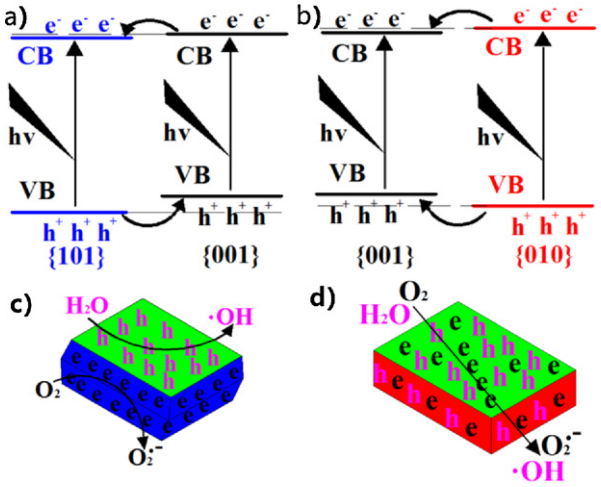


**Scheme 2.** (a) Electronic band structures of {1 0 1}–{0 0 1}; (b) electronic band structures of {0 1 0}–{0 0 1}; (c) electrons and holes distributing of {1 0 1}–{0 0 1}; and (d) electrons and holes distributing of {0 1 0}–{0 0 1}.

Thirdly, the different exposed facets with different arrangement and coordination of the surface atoms which also can affect the adsorption condition of $O_2$ and $H_2O$, and the absorbability of them affect the active oxygen production. Theoretically, the facets with a higher percentage of undercoordinated Ti5c atoms are usually more reactive for •OH production [4,9], because the density of surface undercoordinated Ti5c atoms dominate the surface's ability to adsorb dissociative water. But our photocatalytic results showed that the replacement of {1 0 1} (50% surface undercoordinated Ti5c atoms) by {0 1 0} (100% surface undercoordinated Ti5c atoms) facets inhibits the photocatalytic activity of anatase $TiO_2$ for •OH production. It indicated that the separation efficiency of photogenerated electron–hole is more important than the adsorption condition of $H_2O$ for •OH production. On the other hand, it had been reported that {0 0 1} and {1 0 1} facets displayed different surface-structure sensitivity of $O_2$ activation. More $O_2$ was consumed via multi reduction to form •OH on the {0 0 1} facet than on the {1 0 1} facet upon converting an equal amount of terephthalic acid [36] {0 1 0} facet may show same surface-structure sensitivity of $O_2$ activation like {0 0 1} facets to enhance the multi reduction to form •OH due to they are 100% unsaturated Ti5c atoms. So, the replacement of {1 0 1} by {0 1 0} facets can increase the multi reduction to form •OH, and the NBT concentration changes corresponding to the $O_2^{\bullet-}$ production was just 4 times while TAOH formation on 101/001–1 was approximately 8 times larger than that on 010/001–1 photocatalysis (Fig. 4).

## 4. Conclusion

In this investigation, {1 0 1}–{0 0 1} and {0 1 0}–{0 0 1} anatase $TiO_2$ samples were synthesized, in which two kinds of facet coexist. By comparing the photocatalytic oxidation and reduction activity of {1 0 1}–{0 0 1} and {0 1 0}–{0 0 1} samples, we firstly found that the replacement of {1 0 1} by {0 1 0} facets inhibited the photocatalytic activity of anatase $TiO_2$. The mechanism was examined by PL spectrum, SEM images of selected deposition of Ag, and CB and VB energy level. $TiO_2$ with {1 0 1}–{0 0 1} facets show an enhanced photocatalytic activity due to the efficient charge separation between {1 0 1} facets and {0 0 1} facets. When {1 0 1} facets were replaced by {0 1 0} facets, the photoinduced electrons and holes cannot be well separated, the photocatalytic activity of anatase $TiO_2$ was inhibited.

## Acknowledgements

This work was supported by National Natural Science Foundation of China (No. 21273164) and open foundation of key laboratory of catalysis and materials science of the state ethnic affairs commission and ministry of education, South-central University for Nationalities.

## Appendix A. Supplementary data

Supplementary data associated with this article can be found, in the online version, at http://dx.doi.org/10.1016/j.apcatb.2012.12.043.

## References

[1] A. Kubacka, M. Fernández-García, G. Colón, Chemical Reviews 112 (2012) 1555–1614.
[2] X. Chen, S.L. Shen, L. Guo, S.S. Mao, Chemical Reviews 110 (2010) 6503–6570.
[3] C. Chen, W. Ma, J. Zhao, Chemical Society Reviews 39 (2010) 4206–4219.
[4] A. Selloni, Nature Materials 7 (2008) 613–615.
[5] Z.Y. Jiang, Q. Kuang, Z.X. Xie, L.S. Zheng, Advanced Functional Materials 20 (2010) 3634–3645.
[6] H.G. Yang, C.H. Sun, S.Z. Qiao, J. Zou, G. Liu, S.C. Smith, H.M. Cheng, G.Q. Lu, Nature 453 (2008) 638–641.
[7] H.G. Yang, G. Liu, S.Z. Qiao, C.H. Sun, Y.G. Jin, S.C. Smith, J. Zou, H.M. Cheng, G.Q. Lu, Journal of the American Chemical Society 131 (2009) 4078–4083.
[8] X. Han, Q. Kuang, M. Jin, Z. Xie, L. Zheng, Journal of the American Chemical Society 131 (2009) 3152–3153.
[9] J. Pan, G. Liu, G.Q. Lu, H.M. Cheng, Angewandte Chemie-International Edition 50 (2011) 2133–2137.
[10] X. Zhao, W. Jin, J. Cai, J. Ye, Z. Li, Y. Ma, J. Xie, L. Qi, Advanced Functional Materials 21 (2011) 3554–3563.
[11] X. Wu, Z. Chen, G.Q. Lu, L. Wang, Advanced Functional Materials 21 (2011) 4167–4172.
[12] G. Liu, J.C. Yu, G.Q. Lu, H.M. Cheng, Chemical Communications 47 (2011) 6763–6765.
[13] H. Yu, B. Tian, J. Zhang, Chemistry – A European Journal 17 (2011) 5499–5502.
[14] D. Zhang, G. Li, X. Yang, J.C. Yu, Chemical Communications 45 (2009) 4381–4382.
[15] G. Liu, C. Sun, H.G. Yang, S.C. Smith, L. Wang, G.Q. Lu, H.M. Cheng, Chemical Communications 46 (2010) 755–757.
[16] T.R. Gordon, M. Cargnello, T. Paik, F. Mangolini, R.T. Weber, P. Fornasiero, C.B. Murray, Journal of the American Chemical Society 134 (2012) 6751–6761.
[17] Z. Zheng, B. Huang, J. Lu, X. Qin, X. Zhang, Y. Dai, Chemistry – A European Journal 17 (2011) 15032–15038.
[18] Q. Xiang, K. Lv, J. Yu, Applied Catalysis B: Environmental 96 (2010) 557–564.
[19] T. Tachikawa, S. Yamashita, T. Majima, Journal of the American Chemical Society 133 (2011) 7197–7204.
[20] T. Tachikawa, N. Wang, S. Yamashita, S. Cui, T. Majima, Angewandte Chemie 122 (2010) 8775–8779.
[21] M.M. Maitani, K. Tanaka, D. Mochizuki, Y. Wada, Journal of Physical Chemistry Letters 2 (2011) 2655–2659.
[22] N. Murakami, Y. Kurihara, T. Tsubota, T. Ohno, Journal of Physical Chemistry C 113 (2009) 3062–3069.
[23] T. Ohno, K. Sarukawa, M. Matsumura, New Journal of Chemistry 26 (2002) 1167–1170.
[24] M.D. Arienzo, J. Carbajo, A. Bahamonde, M. Crippa, S. Polizzi, R. Scotti, L. Wahba, F. Morazzoni, Journal of the American Chemical Society 133 (2011) 17652–17661.
[25] C.T. Dinh, T.D. Nguyen, F. Kleitz, T.O. Do, ACS Nano 3 (2009) 3737–3743.
[26] F. Tian, Y. Zhang, J. Zhang, C. Pan, Journal of Physical Chemistry C 116 (2012) 7515–7519.
[27] Y. Wang, K. Deng, L. Zhang, Journal of Physical Chemistry C 115 (2011) 14300–14308.
[28] L. Ye, J. Liu, C. Gong, L. Tian, T. Peng, L. Zan, ACS Catalysis 2 (2012) 1677–1683.
[29] L. Ye, C. Gong, J. Liu, L. Tian, T. Peng, K. Deng, L. Zan, Journal of Materials Chemistry 22 (2012) 8354–8360.
[30] L. Ye, L. Zan, L. Tian, T. Peng, J. Zhang, Chemical Communications 47 (2011) 6951–6953.
[31] L. Sun, Y. Qin, Q. Cao, B. Hu, Z. Huang, L. Ye, X. Tang, Chemical Communications 47 (2011) 12628–12630.
[32] Y.P. Xie, G. Liu, L. Yin, H.M. Cheng, Journal of Materials Chemistry 22 (2012) 6746–6751.
[33] Y.F. Li, Z.P. Liu, L. Liu, W. Gao, Journal of the American Chemical Society 132 (2010) 13008–13015.
[34] J. Lu, Y. Dai, H. Jin, B. Huang, Physical Chemistry Chemical Physics 13 (2011) 18063–18068.
[35] T. Tachikawa, T. Majima, Chemical Communications 48 (2012) 3300–3302.
[36] Y. Zhao, W. Ma, Y. Li, H. Ji, C. Chen, H. Zhu, J. Zhao, Angewandte Chemie 124 (2012) 3242–3246.